3-Phase Hierarchical Graphene-based Epoxy Nanocomposite Laminates for Automotive Applications

Ahmed Elmarakbi[1,*], Panagiotis Karagiannidis[2], Alessandra Ciappa[3], Franco Innocente[3], Francesco Galise[4], Brunetto Martorana[4], Francesco Bertocchi[5], Francesco Cristiano[5], Elvira Villaro Ábalos[6] and Julio Gómez [7]

[1]*Department of Mechanical and Construction Engineering, Faculty of Engineering and Environment, Northumbria University, Newcastle NE18ST, United Kingdom*

[2]*School of Engineering, Faculty of Technology, University of Sunderland, Sunderland SR6 0DD, United Kingdom*

[3] *Delta-Tech S.p.A., località Rifoglieto 60/a - int.1, 55011 Altopascio (LU), Italy*

[4]*Fiat Research Center, via ex Aeroporto 80038 Pomigliano d'Arco (Naples), Italy*

[5] *Nanesa srl, Via Del Gavardello 59/c 52100 Arezzo (AR), Italy*

[6]*Instituto de Tecnologías Químicas Emergentes de La Rioja, Antonio de Nebrija, 8, 26006 Logroño, Spain*

[7]*Avanzare Innovacion Tecnologica S.L. Avda. Lentiscares 4-6 26370, Navarrete, Spain*

*Corresponding author: Ahmed Elmarakbi (ahmed.elmarakbi@northumbria.ac.uk)

Keywords: Graphene, Carbon fibre reinforced polymer (CFRP), Fracture toughness, Shear lap joints

ABSTRACT

Two different types of graphene flakes were produced following solution processing methods and dispersed using shear mixing in a bifunctional (A) and a multifunctional (B) epoxy resin at a concentration of 0.8 and 0.6 wt% respectively. The graphene/epoxy resin mixtures were used to impregnate unidirectional carbon fibre tapes. These prepregs were stacked (seven plies) and cured to produce laminates. The interlaminar fracture toughness (mode-I) of the carbon fiber/graphene epoxy laminates with resin B showed over 56% improvement compared with the laminate without graphene. Single lap joints were prepared using the laminates as adherents and polyurethane adhesives (Sika 7666 and Sika 7888). The addition of graphene improved considerably the adhesion strength from 3.3 to 21 MPa (sample

prepared with resin A and Sika 7888) highlighting the potential of graphene as a secondary filler in carbon fibre reinforced polymer composites.

1. INTRODUCTION

The increasing demand for high-performance lightweight composite materials from different industries i.e. automotive [1][2], aerospace [3][4], marine [5][6], construction [7] and health [8], have stimulated an expanding development of carbon fibre reinforced polymer (CFRP) composite materials. CFRP composites consist of carbon fibres (CF) reinforcing agent dispersed in a polymer matrix which is a thermoset or a thermoplastic polymer [9]. Epoxy thermosetting polymers are preferred, instead of thermoplastics, due to their lower viscosity, which makes them easier to process and combine with long and continuous CF reinforcements [9]. CF are lightweight, stiff, and strong (density ρ =1.78-2.15 g/cm^3, elastic modulus E=230-725GPa, tensile strength TS=1.5-4.5GPa [10]), which provide most of stiffness and strength of CFRP. The CF are impregnated with the thermosetting liquid resin which is partially cured (prepreg) [9]. Prepregs are stacked one after another to prepare composite laminates. A major drawback and life-limiting failure mechanism of CFRP composite laminates is their tendency for crack initiation, propagation, and interlaminar delamination [11][12][13]. Also, compared to the outstanding in-plane properties of composite laminates, the out-of-plane properties of these materials are less impressive. Consequently, it is critical to improve interlaminar mechanical properties of CFRPs such as the interlaminar fracture toughness (G_{IC}) [14].

Different micro-fillers or nanoparticles such as dendritic hyperbranched polymers [15]; carbon nanotubes (CNTs) [16] [17]; inorganic particles [18], [19] or rubber [20] have been used for toughening epoxies. These additives although they are used in composite manufacturing they come with several drawbacks such as decrease of the glass transition temperature (T_g) and modulus and resin viscosity (η) increase [20]. More recently, graphene has attracted significant attention as a reinforcement of polymer matrices due to its excellent electrical and mechanical properties [21] and potential for low cost mass production [22][23][24]. Most of the studies focused on the effect of graphene oxide (GO) [25][26], functionalised graphene flakes [27][28], as a primary reinforcement of epoxy matrices without inclusion of CF. Fewer reports refer to three-phase composite laminates i.e. graphene/CF/epoxy which are widely employed in varieties of applications. Kostagiannakopoulou et al. [29] dispersed graphene nanoplatelets (GNPs) and GO in epoxy

using three-roll milling and prepared multilayer laminates consisting of 12 neat epoxy and 4 graphene-modified layers in the middle of the laminate. They showed a 50% increase in the total G_{IC} of the laminates although no significant increase was observed in the initial G_{IC} which is related to the matrix toughness. Ning et al. [30] incorporated a GO reinforced epoxy (bisphenol-F) interleaf into the interface of CFRP laminates and found an increase of 170% in the G_{IC}. Ref [31] passivated GNPs with hydrogen to improve exfoliation and dispersion of the GNPs into a bisphenol-F epoxy and found 48% improvement in the initial G_{IC} after the addition of 0.5%wt of GNPs in the laminates.

In this work, we produced two new types of pristine graphene flakes of different lateral size and thickness following solution processing methods and disperse these flakes into a bifunctional (epoxy A) and a multifunctional epoxy resin (epoxy B) both based on bisphenol A. Both resins have relatively low η providing good processability and high T_g assuring operational stability which makes them suitable for different automotive applications. The graphene/resin mixtures were used to impregnate unidirectional CF following a hot melt impregnation process. To prepare the laminates in this work, we used seven layers of CF sheets (plies) stacked one after another with the same orientation and impregnated all with graphene-doped resin. Mechanical tests performed showed an increase in the initial G_{IC} by 56.3% due to the addition of graphene.

Finally, we studied the adhesive bonding of the prepared laminates (adherents) using two different polyurethane adhesives. Adhesive bonding is considered as the main joining technology in automotive construction [32]. It is a process whereby an adhesive is placed between the parts (adherents) where it serves as the material that joins the substrate and transmits the load through the joint. The principal benefits deriving from the use of adhesive joining include low cost, design flexibility, improved stiffness of the joint, ability to damp noise and vibrations and possibility to join dissimilar materials [33]. Compared to mechanical fastened joints, adhesive bonding joints are relatively lighter, with comparatively lesser stress concentrations and much-improved fatigue lives [34]. The single lap-joint specimens prepared using graphene/CF/epoxy laminates jointed by polyurethane adhesives showed a significant improvement in the lap joint shear strength owing to the presence of graphene.

2. EXPERIMENTAL

2.1. Materials

The epoxy systems were developed and provided by Delta-Tech (Dtech) from Italy, termed as epoxy 'A' (EM120, bifunctional) and epoxy 'B' (EM180, multifunctional). Epoxy A has a T_g of ca. 120^{o}C after curing while epoxy B has a T_g of ca. 180^{o}C after curing. Expandable graphite intercalated with sulfuric and nitric acid were sourced by Faima Luh and natural graphite with 300 mesh particle size was sourced by Grafitos Barco S.A. CF unidirectional tapes 600mm wide, having 150g/sqm fibre areal weight (150-UTS50, F13, UD) were obtained from Tenax Europe. The CF have a TS of 5100 MPa, E of 245 MPa, and ρ of 1.78 g/cm^3. For shear lap joints testing the SikaForce-7666 and SikaForce-7888 adhesives were obtained from Sika.

2.2 Preparation and characterisation of the graphene flakes

Nanesa Srl from Italy microwaved expandable graphite (Faima Luh) for 12 s at 2 kW which caused expansion into a worm-like structure. The expanded graphite was then dispersed in deionised water, without surfactants, at a concentration of 3.75 g/L and ultrasonicated for 1 h using a tip sonicator working at a frequency of 20 kHz and delivering a power of 1000 W. Following exfoliation, the dispersion was vacuum filtered and the powder was collected. These graphene flakes are termed as Gr-NAN.

Avanzare Innovaccion Technologica from Spain prepared another type of graphene (named Gr-AVA) starting from natural graphite (Grafitos Barco S.A.). A water dispersion of graphite/polyvinylpyrrolidone (PVP) /water (1:1:50) was agitated using a rotor stator for 12h and then ultrasonicated using a tip sonicator Hielcher UP400S/H40 for 12h. The mixture was decanted to remove the non-exfoliated material. The exfoliated flakes were collected from the supernatant and then centrifugated at 4000 rpm for 12 hours to be collected as a wet solid. The wet solid was washed two times with water to remove PVP, then dispersed in osmotic water and centrifugated at 4000 rpm for 15min two times. The solid was dried in a vacuum oven for 14 h at 130 ºC, obtaining a final yield of 18%.

Scanning Electron Microscopy (SEM) was utilised to assess the lateral size and morphology of the graphene flakes. SEM was performed using an EVO MA10 Zeiss operated at 10 kV and a Hitachi S-2400 operated at 18 kV both in secondary electron imaging mode. Energy Dispersive X-ray Spectrometry (EDS) was performed in Back Scattered Electron (BSE) mode using INCA software for elemental analysis. Samples were dispersed in isopropanol and sonicated with a Hielscher UP200S sonicator for 15 minutes and then placed on copper

foils for imaging. High-Resolution Transmission Electron Microscopy (HRTEM) images were acquired using a HT7800 RuliTEM Hitachi operated at 120 kV and a JEM-2010 (JEOL, Japan) operated at 120 kV. Samples for HRTEM imaging were prepared onto TEM carbon grids. X-ray diffraction measurements were performed using an automatic Bruker D8 Advance diffractometer, in reflection, at 35 KV and 40 mA, using the nickel-filtered CuKα radiation (1.5418 Å) with a range of 2θ=10-100º. The average crystallite size was calculated from the line broadening of the diffractogram peaks using Scherrer formula (Eq.1).

$$D = \frac{K\lambda}{B\cos\theta_B} \quad (1)$$

where D is the average crystallite size, K is a coefficient taken to be 0.89 according to Raza et al.[35], λ is the incident X-ray wavelength, B is the full width half maximum (FWHM) of the diffraction peak expressed in radians; and θ_B is the peak position.

2.3 Preparation of graphene/epoxy resin mixture (2-Phase Composites)

Dispersion of graphene flakes into epoxy systems was performed by adding the graphene flakes directly into the resins using high shear mixing. Dispersion was performed by a two-step process; a first step with a shaft dispersion system with cowless blades at 2000 rpm for 60 min followed by a second step of homogenisation with a Silverson high shear mixing system at 3000 rpm for 30 min. Following this protocol, Gr-NAN flakes were added into resin A at 0.8 wt% (sample A-0.8Gr-NAN) and into resin B at 0.6 wt% (sample B-0.6Gr-NAN). Higher graphene content led to limited workability to hot melt impregnate the resin/graphene mixture into CF tapes. Also, samples were prepared using Gr-AVA (samples A-0.8Gr-AVA and B-0.6Gr-AVA). After the dispersion of the graphene flakes suitable catalysts and accelerators were added using a laboratory mixer under vacuum for the curing of the resins. These products characterised as prepregs are susceptible to spontaneous crosslinking at ambient conditions, therefore, to extend the time of use, the said materials were stored at -18° C.

2.4 Curing study of resins and graphene/epoxy resin mixtures by η measurements, and Differential Scanning Calorimetry (DSC)

Measurements of η were performed using a DHR-1 (TA Instruments) rheometer equipped with electrically heated parallel plates (heating rate 2°C/min). DSC was carried out in order

to determine the curing time, the rate of reaction, the enthalpy and the T_g of the resins with and without graphene. DSC measurements were performed using a DSC-1 (Mettler Toledo) according to ASTM E2160-04 (enthalpy determination) and to ASTM D3418-08 (T_g determination). The measurements were performed as follows: i) isothermal: 1 min at -40°C; ii) temperature was ramped from -40 to 250°C at 10°C/min; iii) cooling down from 250°C to 25°C at -20°C/min; iv) isothermal: 1 min at 25°C; and v) temperature ramp from 25°C to 250°C at 20°C/min.

2.5 Dynamic Mechanical Analysis (DMA) of cured resins and graphene/resin composites

DMA tests were performed using a DMA Q800 (TA Instruments) equipped with single cantilever clamp according to ASTM D7028 (frequency of 1Hz, heating rate of 5°C/min). Samples for DMA characterisation were prepared as follows; neat resins and graphene resin mixtures were poured into an aluminium mould. The mould was placed into a vacuum bag and the pressure was reduced by means of a vacuum pump. The mould was transferred into an autoclave for curing. Resin A based samples were cured for 90 min at 120°C (3 bar) and resin B based samples were cured for 90 min at 135°C (3 bar) followed by a second heating for 120 min at 180°C with a heating rate of 1°C/min.

2.6 Hot melt impregnation of unidirectional carbon fibres tapes with neat epoxies and graphene/epoxy mixtures (3-Phase Composites)

Five laminate samples were prepared by impregnating CF; two with neat resins (A and B) and three with resins containing graphene. These samples were termed as CF-A-neat; CF-A-0.8Gr-NAN; CF-A-0.8Gr-AVA; CF-B-neat; and CF-B-0.6Gr-NAN. The resin systems, were hot melted and coated on special paper substrates. The coating resin amount (g/sqm) was tuned to obtain the defined resin content of 36% by weight in the prepregs. Seven layers of carbon fibre sheets (plies) were stacked one after another with the same orientation with resin layers applied between them. The prepregs were cured under vacuum in autoclave at a pressure of 6 bars. The samples were heated with a heating rate of 2°C/min up to 120°C for resin A and 180°C for resin B and heated isothermally for 90min.

2.7. Mode I Interlaminar Fracture Toughness (G_{IC}) of graphene/CF/epoxy matrix laminates

The determination of Mode I (tension loading) interlaminar fracture toughness G_{IC} of unidirectional carbon fiber/graphene/epoxy matrix laminates was performed according to the ASTM D5528 standard, using double cantilever beam (DCB) specimens and tested with an electromechanical universal MTS Criterion model 45 system equipped with a load cell of 100 kN. Once the unidirectional laminates were prepared, DCB rectangular specimens were cut 125 mm long and 20 mm wide containing a non-adhesive insert (13µm thick and 63mm long) on the midplane that serves as a delamination initiator. This distance corresponds to an initial delamination length (a_0) of approximately 50 mm plus the extra length required to bond the hinges or load blocks (Figure 1.a).

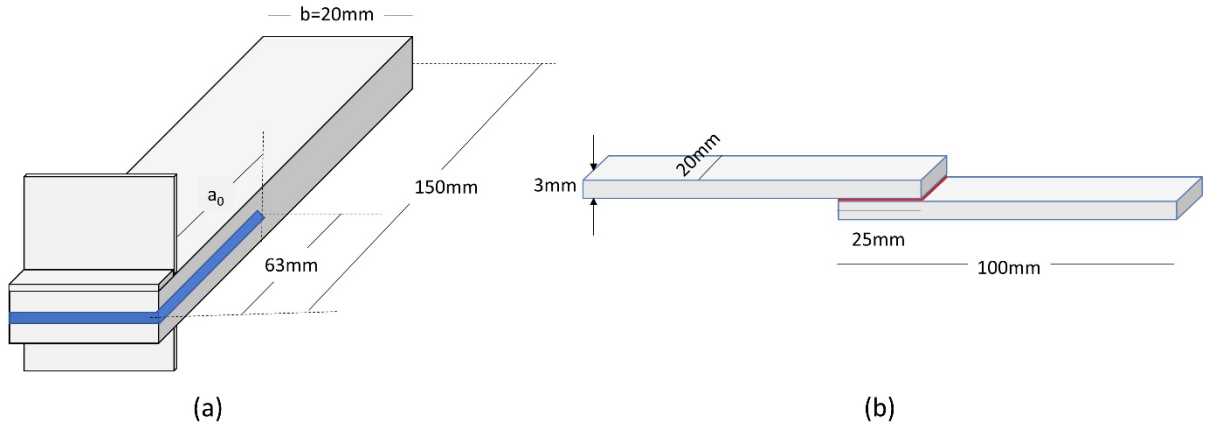

Figure 1. Schematics of a) double cantilever beam specimen used for interlaminar fracture toughness characterization and b) geometry and dimensions of the single lap joints.

2.8 Shear lap joints

The prepared laminates were used as adherents to prepare shear lap joints. In order to prepare the joints with high accuracy and precise adhesive thickness, the substrates were cut using water-jet technology and joints were realized using a template control made of steel. The surface of the substrates to be joined were treated with sandpaper to eliminate possible processing residues and to roughen the surfaces for better adhesion after degreased with heptane soaked wipes. The joint dimensions were in accordance with the FCA standard, with a bonding layer thickness of 1 mm. A schematic of the lap joint is shown in Figure 1.b. Lap shear adhesion tests were performed at room temperature (23°C ± 2°) using a tensile machine with a crosshead rate motion of 13 mm/min. The joints were characterised according to the ASTM D5868 standard.

3. RESULTS AND DISCUSSION

3.1 Characterisation of graphene flakes.

The lateral size of the graphene flakes produced were first determined using SEM. Typical SEM images of the Gr-NAN and Gr-AVA flakes are presented in Figure 2.a and 2.b respectively. Scans obtained from Gr-NAN samples revealed flakes in the range of 15-30 μm while scans from Gr-AVA samples showed flakes of 1-2 μm (Table 1). The thickness of the flakes was determined using HR-TEM and XRD. In HR-TEM the edge of the flakes is measured which can be positioned out-of-plane ('curled up') even when deposited in-plane on a flat surface. The thickness of the flakes is estimated from the thickness of the edge of the flakes sticking out of the plane of the grid [36]. HR-TEM measurements showed a typical thickness of 14nm for Gr-NAN flakes and 3-4nm for Gr-AVA (Figures 2.c and 2.d respectively).

The XRD spectra obtained from both samples exhibited a peak at $2\theta=26.4°$, a basal reflection (002) which corresponds to a d-spacing of 0.34 nm and represents the interlayer distance. An average Z-dimension or thickness of 10.78nm was obtained for Gr-NAN which corresponds to 32 layers while the Z-dimension or thickness was 3.06 nm for Gr-AVA corresponding to 9 layers Elemental analysis was performed to determine the oxygen content on the graphene powders. EDS analysis showed a ratio of C_{1s}:O_{1s} of 44:1 significantly larger that the ratio typically found in GO (~2-3 [37][38][39]) indicating that the Gr-NAN flakes are pristine. XPS analysis performed on Gr-AVA showed a ratio of C_{1s}:O_{1s} of 101:1 which shows that both graphene flakes produced are pristine. The above results are summarised in Table 1.

Table 1. Characteristic properties of the graphene flakes used.

	Gr-NAN	**Gr-AVA**
Lateral size (μm)		
SEM	15-30	1-2
Thickness		
TEM (nm)	14	3-4
XRD (Number of Layers)	32	9
Elemental analysis (C:O)		
EDS	44:1	NA
XPS	NA	110:1

NA: Not available data

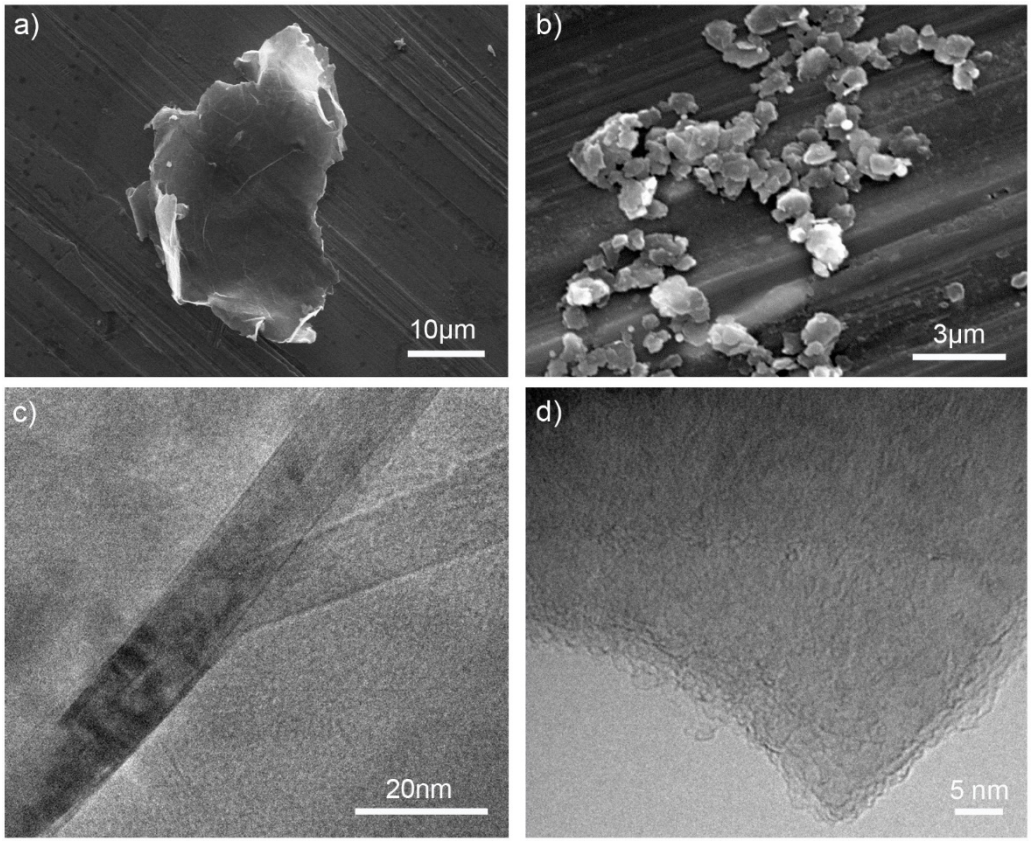

Figure 2. SEM images of typical flakes a) Gr-NAN and b) Gr-AVA and HR-TEM images showing a typical flake thickness of c) 14nm for Gr-NAN and d) 3-4nm for Gr-AVA.

3.2 Rheological and DSC curing study of neat resins and graphene/resin mixtures

As the curing process of the epoxy matrix is critical in defining the materials properties of the epoxy composites it is essential to investigate the curing process of neat resins and the influence of the addition of graphene flakes. Epoxy resins are defined as low-molecular-weight pre-polymers containing more than one epoxide group of the form shown in Figure 3a. Di-Glycidyl Ether of Bisphenol A (DGEBA) is a bifunctional epoxy resin, that contains two epoxy groups (Figure 3b); however trifunctional and tetrafunctional epoxy resins have been prepared [40]. Curing is the reaction process of the epoxy groups mainly with the amino groups of a hardener (Figure 3c).

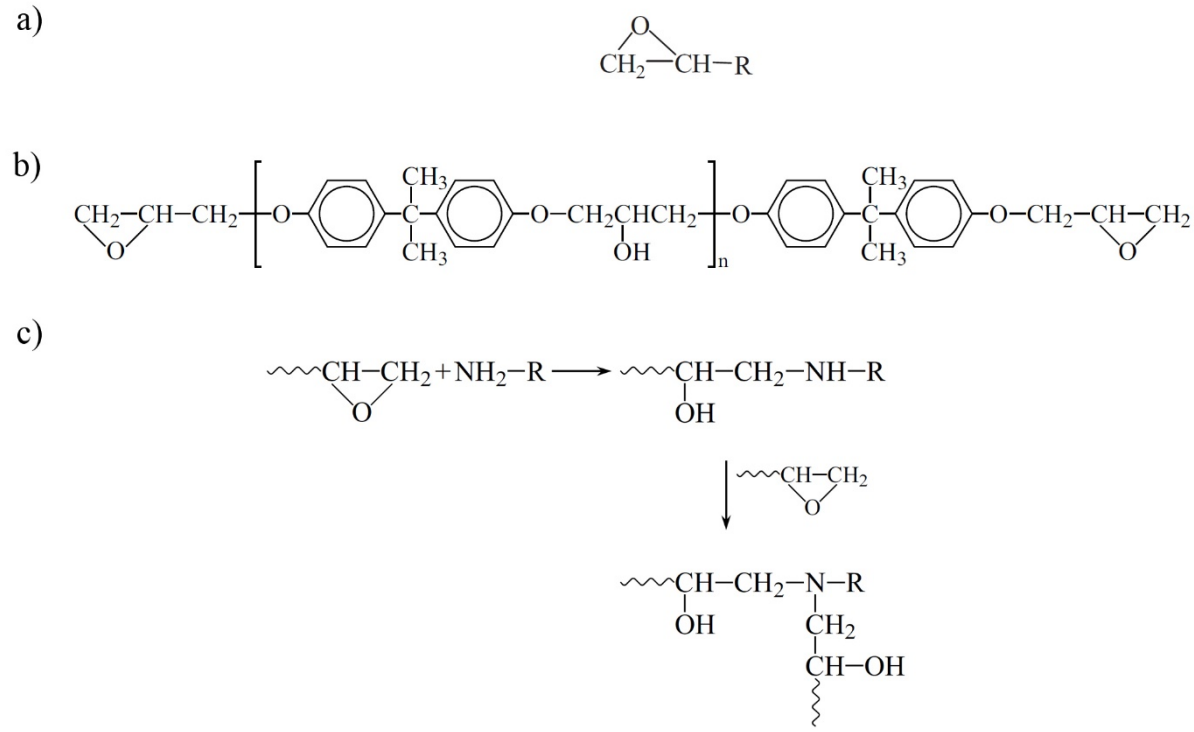

Figure 3. a) The epoxide group, b) the chemical structure of Di-Glycidyl Ether of Bisphenol A (DGEBA) and c) cure reaction mechanism of amine and epoxide [40].

First, curing was followed by η measurements of the neat resins upon a temperature ramp (2°C/min) from room temperature (RT) to 140°C. At 60°C resin A showed η of 41 Pa·s while resin B showed a higher η of 49 Pas. As shown in Figure 4, η of resin A typically drops due to temperature increase and it increases due to curing as the material hardens. Thus, a minimum η of 0.7 Pa·s is obtained at 107°C for resin A as presented in Table 2. From this point η grows exponentially, with an initial average rate of ca. 12 Pa·s/°C, an index of the speed of crosslinking. The addition of 0.8 wt% of Gr-NAN increases the viscosity to 200 Pas at 50°C and 77 Pa·s at 60°C. The curing rate also increases to 15 Pa·s/°C. The addition of Gr-AVA increases η values without affecting the curing rate.

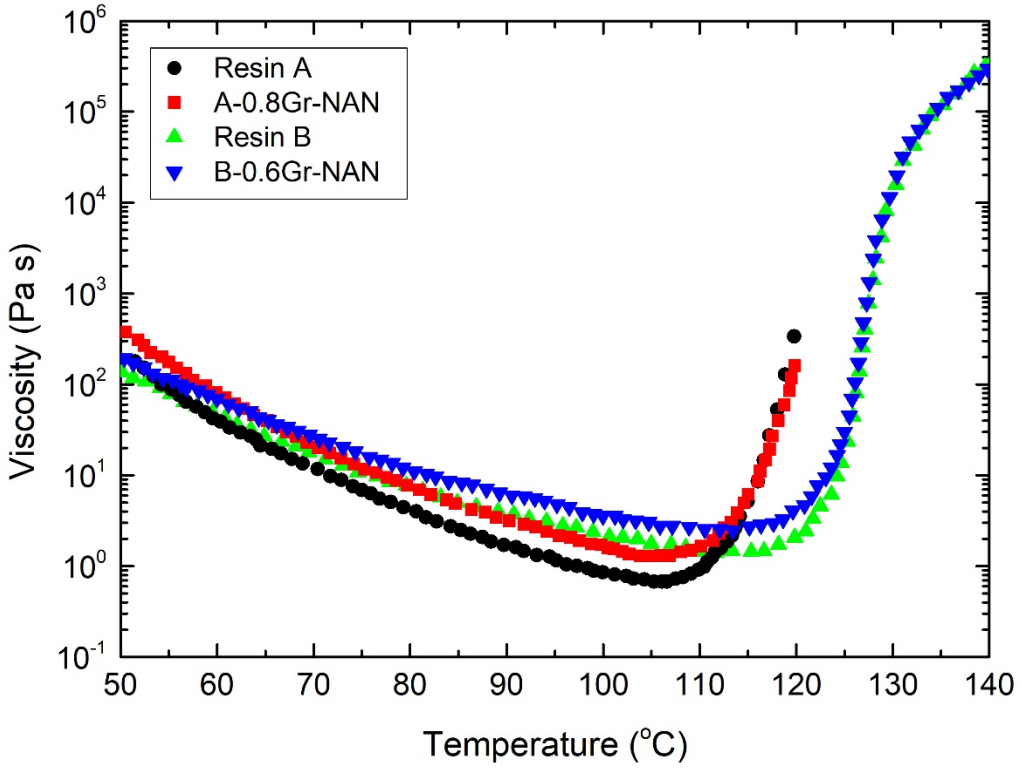

Figure 4. Viscosity as a function of curing temperature for resin A, sample A-0.8Gr-NAN, resin B and sample B-0.6Gr-NAN.

Table 2 presents the η values recorded at 60°C, the minimum viscosity values obtained during temperature ramp as well as the curing rate. Resin B shows a higher viscosity of 49 Pa·s at 60°C, a higher minimum value of 1.1 Pa·s at 114°C and a lower curing rate of 10 Pa·s/°C. The addition of Gr-NAN graphene flakes increases the η values to 68 Pa·s at 60°C and the curing rate to 12.5 Pa·s/°C.

Table 2. Viscosity at 60°C, minimum viscosity values and curing rate.

Sample	**Viscosity (Pa·s) at 60°C**	**Minimum viscosity (Pa·s) / (temperature)**	**Curing rate (Pa·s/°C)**
Resin A	41	0.7 (107°C)	12
A-0.8Gr-NAN	77	1.1 (105°C)	15
A-0.8Gr-AVA	50	1.1 (106°C)	11
Resin B	49	1.1 (114°C)	10
B-0.6Gr-NAN	68	2 (115°C)	12.5

Curing was also followed by DSC measurements. The reactivity parameters, onset and peak curing temperature, enthalpy upon curing, and ultimate T_g (after curing) were determined. Curing is observed as a large exothermic peak. The onset of curing is the temperature at which heat flow deviates from a linear response and the exothermic peak temperature reflects the maximum rate of curing. The area under the exothermic peak can be integrated to give the heat of cure (ΔH_{cure}). The onset and peak temperatures of curing, the curing enthalpy and the T_g of the cured resin are listed in Table 3. The addition of graphene flakes has no effect on the onset and peak temperatures. Also, no significant changes are observed in the curing enthalpy and the cured T_g for resin A. However, in the case of resin B an increase of 15 J/g in the enthalpy is observed which indicates a higher degree of curing which reveals a higher degree of crosslinking density. Recently Aouf et al. [41] synthesized a multi-functional epoxy resin; the cured epoxy resin showed a higher cross-linking density than DGEBA cured under the same conditions in accordance with our results. This is confirmed with a 8°C increase in the cured T_g. This shows a positive enhancement effect which is typical for rigid fillers and consists an advantage over soft fillers (e.g. thermoplastic particles, rubber, etc.) which reduce the T_g [42].

Table 3. DSC results obtained for all examined materials

Sample	**Onset (°C)**	**Peak (°C)**	**Enthalpy (ΔH J/g)**	**Cured T_g (°C)**
Resin A	128,4	138,6	-350	110
A-0.8Gr-NAN	128,3	139,2	-349	110
A-0.8Gr-AVA	128,6	138,8	-342	110
Resin B	135,6	147,6	-479	186
B-0.6Gr-NAN	135,3	147,5	-494	194

3.3. DMA study of cured resins and graphene/resin composites.

DMA spectra of neat A and B resins and in the presence of Gr-NAN are presented in Figure 5a and 5b respectively showing the storage modulus (E') and tanδ (= loss/storage modulus =E''/E') versus temperature. Table 4 summarises the values obtained for E' onset (calculated as the temperature at intersection of tangent lines from the storage modulus) and tanδ peak

both related to T_g. E' onset occurs at the lowest temperature and relates to mechanical failure, while tanδ peak occurs at the highest temperature and is most often used because it is more accurately determined [43]. Resin A shows an E' onset value of 143.2°C while the resin B shows a higher E' value of 179.9°C. Similarly resin A shows a tanδ peak of 150.3°C while resin B has a tanδ peak at 204.2°C indicating that resin B has higher curing degree and crosslinking density. It is evident that the addition of graphene flakes (Gr-NAN or Gr-AVA) have no effect on the T_g values of resin A. On the contrary the addition of graphene flakes (Gr-NAN) in resin B increases E' onset 19°C, and tanδ peak 13°C.

Table 4. T_g values determined by DMA for all examined materials

Graphene epoxy composites	**E' on set (°C)**	**tanδ peak (°C)**
Resin A	143.2	150.3
A-0.8Gr-NAN	142.8	149.9
A-0.8Gr-AVA	143.6	150.5
Resin B	179.9	204.2
B-0.6Gr-NAN	198.9	217.2

It is known that a high tan δ peak indicates high molecular mobility and so less crosslinking density [44]. The maximum height of the tan δ peak of resin A is 0.84 while that of resin B it is 0.31 which implies that resin B has higher crosslinking density. From the width of the tan δ curve it can be observed that the glass transition temperature region spreads over a wide temperature range. This extended transition region is a result of high degree of structural heterogeneity of the sample. The broader tan δ peak implies a more heterogeneous network with a wide distribution of relaxation times [45] [46]. Qualitatively this structural heterogeneity is observed by measuring the peak width at half its height of the tan δ curve as shown in Figure 5. Resin A tanδ peak has a FWHM of ΔT=15.88 (°C) while Resin B has ΔT=39.7 (°C). Hence resin B has higher structural heterogeneity and crosslinking density in agreement with DSC results.

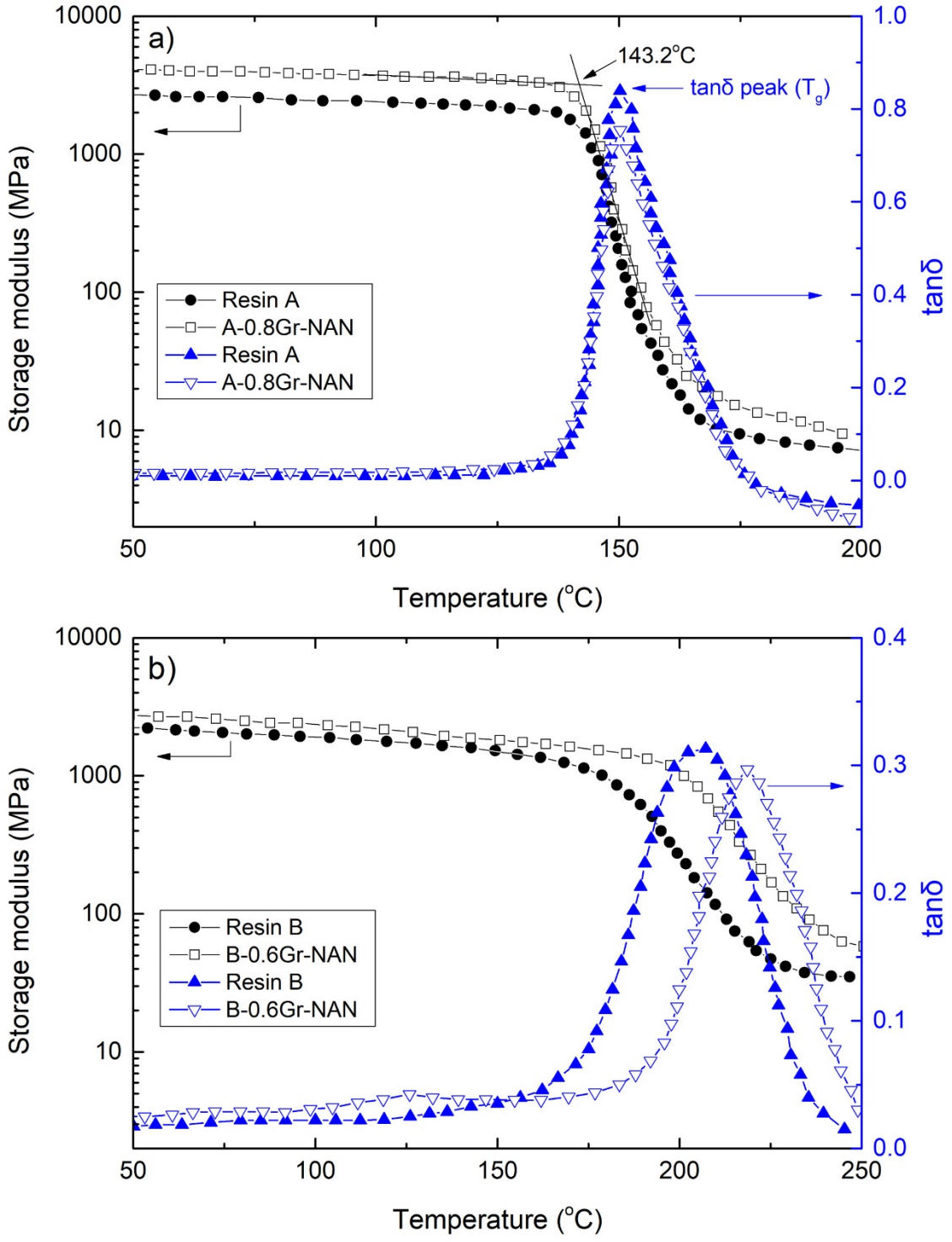

Figure 5. DMA storage modulus and tanδ versus temperature of a) Resin A and A-0.8Gr-NAN and b) Resin B and B-0.6Gr-NAN.

The positive effect of graphene on curing of resin B must be due to its better wetting by the resin and/or to the presence of functional groups in resin structure which form chemical

bonds and/or secondary Van der Waals bonds such as hydrogen bonds with the graphene surface functional groups [47].

3.4 Mechanical Testing of three-phase composites

Interlaminar fracture toughness (Mode-I)

The Mode-I DCB theory was used to study the delamination resistance of the prepared three phase composites. Force-displacement curves from the DCB tests of the different group of neat and graphene/CF modified matrix composites are shown in Figure 6. In all samples, the load values increased up to a maximum level almost linearly within the elastic region. This initial linear response is followed by a sudden decrease in load which corresponds to the initial crack propagation from the starter crack (where the non-adhesive material inserts ends). It is also observed that the maximum load at the initiation point is followed by a gradual load decrease as the crack propagates further.

The initiation fracture energy is more directly related to matrix toughness and does not involve any fibre bridging mechanisms [29]. This is due to the fact that the first increment of delamination appears at the end of the non-adhesive film and the interlaminar epoxy matrix has not still developed the full interaction with the fiber reinforcement (cohesive failure). Table 5 shows that resin A presents an interlaminar fracture toughness, (G_{IC}) of 0.36 kJ/m^2 higher than resin B which shows 0.16 kJ/m^2. Resin B has a higher crosslinking density than resin A according to DSC and DMA results. High crosslinking density has been correlated by a number of researchers [48][49][50] with a decrease in fracture toughness of pristine epoxy due to internal stresses induced during curing of the epoxy. Within a high cross-link density epoxy, resistance to crack initiation is very low and the void growth due to plastic deformation is constrained.

Figure 6 shows that addition of Gr-NAN graphene in Resin A caused an increase in the ultimate load from 42 N to 46 N while the increase in resin B is significantly higher from 32 N to 42 N. For resin A the interlaminar fracture toughness, G_{IC} increases by 8.3% by the addition of the Gr-NAN flakes while it decreases by 11.1% by the addition of the Gr-AVA (Table 5). Addition of Gr-NAN in resin B caused an increase in G_{IC} by 56.3%. This increase is in accordance to an established view that for matrices with G_{IC} lower than 0.5 kJ/m^2 the addition of reinforcing agents increases the G_{IC} of the composite [19]. The improvement in

resin B (multifunctional) could be attributed to the higher amount of the hydroxyl groups present which can form hydrogen bonds with the low amount of oxygen groups of the graphene flakes.

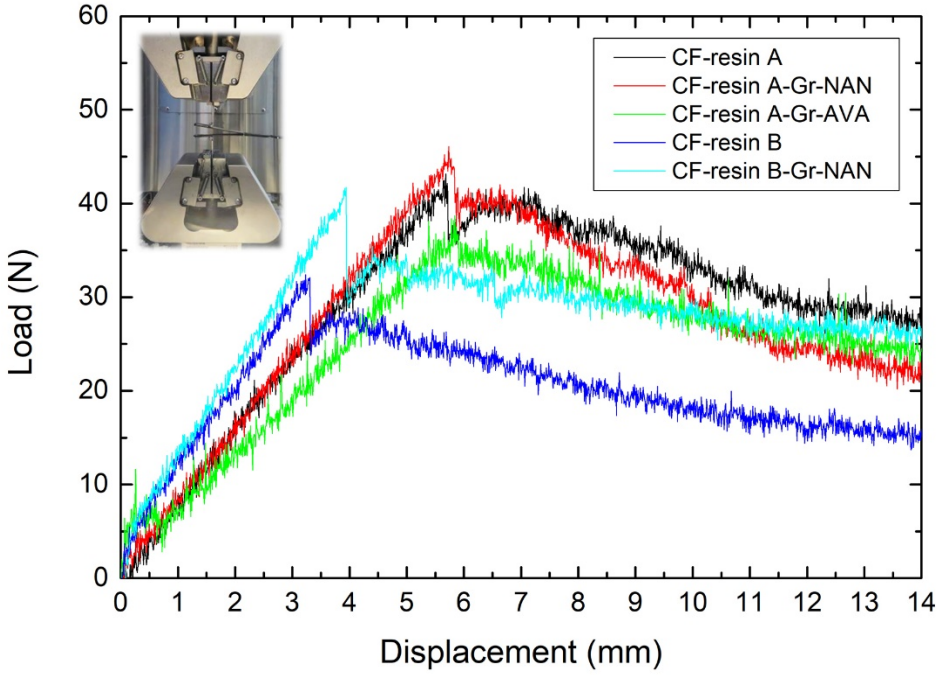

Figure 6. Representative load-displacement curves of the composite specimens under study and DCB test specimen under mode-I loading (inset).

Table 5. Initial interlaminar fracture toughness, G_{IC} of CF/epoxy/graphene laminates under study.

Samples	**G_{IC} (kJ/m^2)**	**% Change**
CF-Resin-A	0.36	-
CF-A-0.8Gr-NAN	0.39	+8.3
CF-A-0.8Gr-AVA	0.32	-11.1
CF-Resin-B	0.16	-
CF-B-0.6Gr-NAN	0.25	+56.3

3.5 Microscopical investigation

In order to understand the mechanisms of failure the fracture surfaces were investigated using SEM. The fracture surfaces from the test specimens prepared with resin A and containing Gr-NAN (a) and Gr-AVA (b) are presented in Figure 7.a and 7.b respectively. It is evident that

sample containing Gr-NAN has increased surface roughness, possibly as a result of the higher lateral flake size, which results in larger matrix plastic deformation yielding higher fracture energy [51]. Studies of fractured surfaces showed that a smooth, featureless surface is attributed to brittle failure, while rougher fracture surfaces are attributed to tougher nanocomposites [52]. Furthermore, the fractured surface of sample CF-A-0.8Gr-AVA clearly shows the presence of micron-size voids, a common type of defects, arising from the manufacturing process [53]. It is suggested that the mechanical properties are negatively affected by increasing porosity which is correlated with the decrease of G_{IC} in the case of the Gr-AVA samples having significantly larger voids. Figure 7.c shows the fracture surface of sample prepared with resin B. The significant improvement in resin B could be attributed to the presence of agglomerates. Additional SEM images of the sample CF-B-0.6Gr-NAN presented in the supplementary information (Figure S2) reveal that graphene is well situated between the fibres. The samples are free of defects e.g. discontinuities or voids, and the fibres present no ‘’pull out’’ from the matrix indicating a strong interface interaction between the fibres and the hybrid matrix [54].

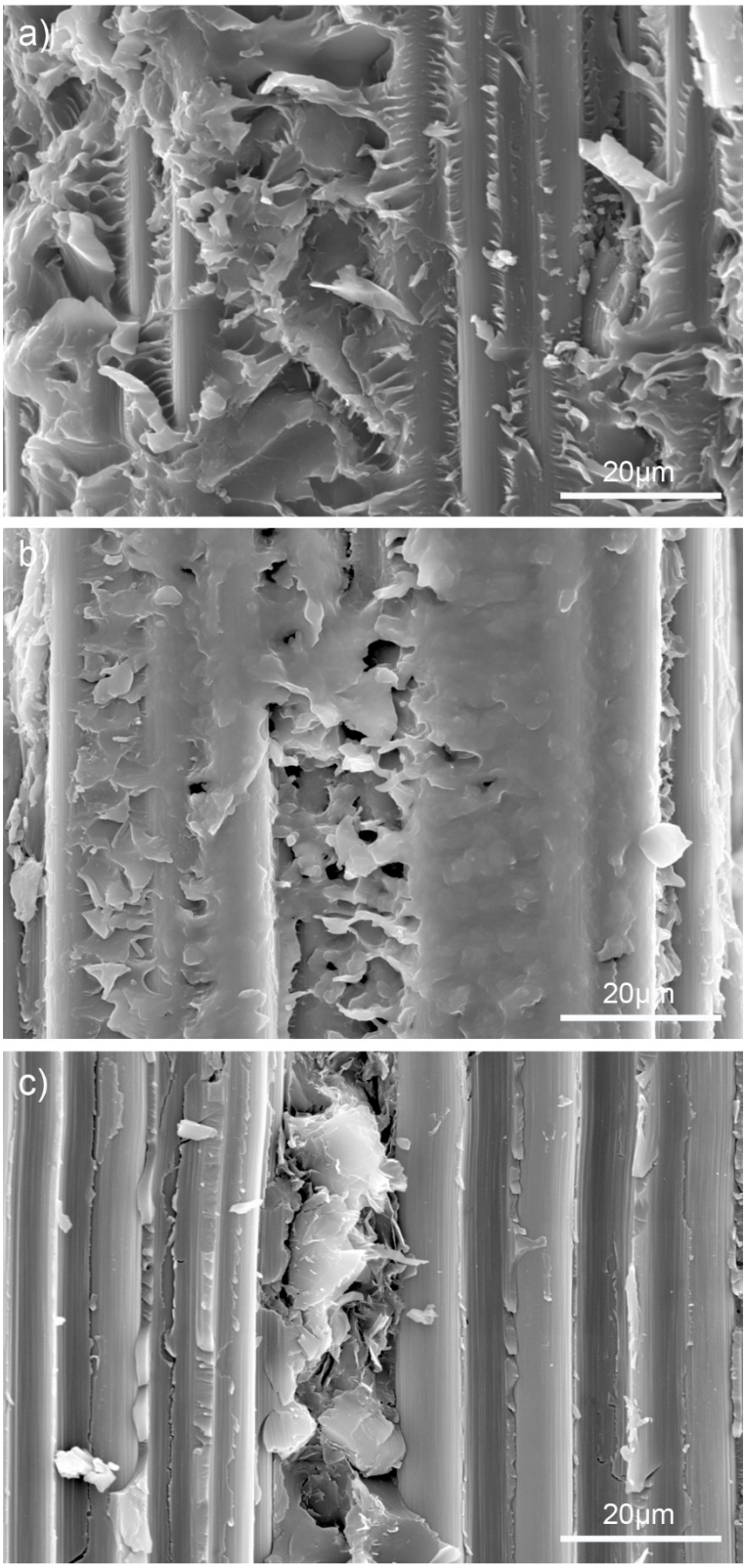

Figure 7. SEM images of fracture surfaces from G_{IC} tests from sample (a) CF-A-0.8Gr-NAN and (b) CF-A-0.8Gr-AVA and (c) CF-B-0.6Gr-NAN

3.6 Performance of adhesives

The effect of graphene on the adhesion properties of CFRP laminates was investigated by preparing shear lap joint speciments using polyurethane Sika 7666 and 7888 adhesives which are two component adhesives. Polyurethanes are made generally by reacting di or poly-alcohols (component A) with di- or poly- isocyanates (component B). Sometimes, component A contains also a diamine, which reacts also with isocyanates to give urea linkages. Component A in Sika 7666 contains a polyol, butane-1,4-diol, a minor amount of diamine and a catalyst. Component A in Sika 7888 contains also a polyol, bisphenol-A-propoxylate a minor amount of diamine and a catalyst. Component B in both adhesives contains mainly 4,4`-Methylenediphenyl diisocyanate. By mixing the two components A and B a polyurethane adhesive is produced (Figure 8a) which contains also urea units (Figure 8b).

a)

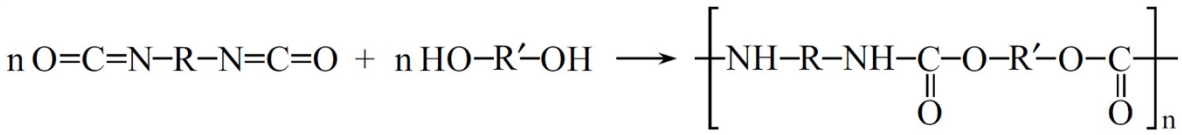

b)

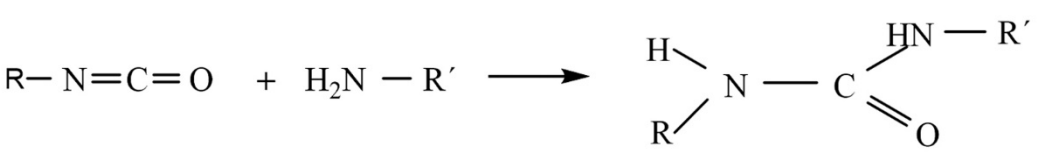

Figure 8. Main chemical reactions which take place during the mixing of component A and component B of Sika 7666 and 7888; production of a) polyurethane adhesive and b) urea units.

Lap shear joints were prepared and tested according to the ASTM D5868 standard test method for lap shear adhesion for fibre reinforced plastic bonding. All samples showed adhesive and cohesive failure; adhesive failure is when the bond failure occurs between the adhesive layers and one of the adherents while cohesive failure is when the bond failure occurs at the adhesive layer [33]. Figure 9.a shows curves obtained from the neat resins with Sika adhesives without graphene. The maximum shear stress was calculated from the peak load divided by the shear area (Table 6). Laminate samples fabricated with resin B demonstrate higher adhesion strength than laminates made of resin A. Multifunctional resin B has more hydroxyl groups available to form hydrogen bond with carbonyl and amino groups of the polyurethane adhesive. Shear lap joints made of Sika 7888 show higher shear strength

in comparison with Sika 7666. Figure 9.b shows that the addition of graphene significantly increase the maximum adhesion strength. The most significant increase was observed in sample made with Sika 7888 where the addition of graphene Gr-NAN increased the adhesion strength from 3.3MPa to 21MPa. The fact that the joints made of CF-A-0.8Gr-AVA adherents did not show such improvements allows us to conclude that probably it is the high lateral size of the Gr-NAN and the induced roughness at the adherent/adhesive interface which improves the adhesion strength of the joint.

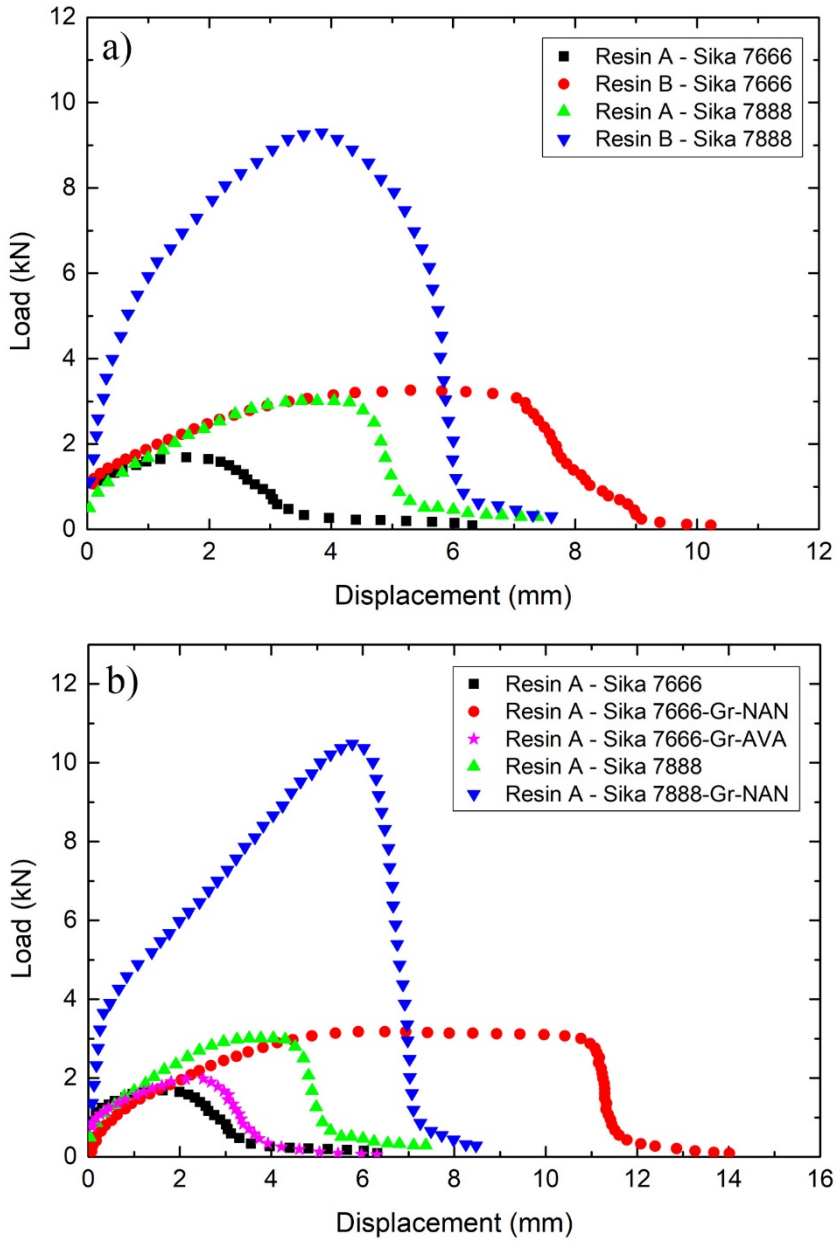

Figure 9. Lap shear tests on joints made of a) neat resins with Sika 7666 and 7888 adhesives and b) resin A with Sika 7666 and 7888 adhesives with and without graphene.

Table 6. Maximum shear stress for the shear lap joints under study.

Sample	Maximum shear stress (MPa)
CF-Resin A - Sika 7666	3.3
CF-Resin B - Sika 7666	6.4
CF-Resin A - Sika 7888	6
CF-Resin B - Sika 7888	19
CF-Resin A - Sika 7666 + Gr-NAN	6.1
CF-Resin A - Sika 7666 + Gr-AVA	4.2
CF-Resin A - Sika 7888 + Gr-NAN	21

CONCLUSIONS

In this work pristine graphene flakes with different lateral size and thickness were produced and added into epoxy resins having different chemical structure, viscosity and T_g. The addition of either graphene flakes increased the viscosity and the curing rate of the resins. The maximum graphene content that allows for impregnation of CF was found to be 0.8% wt (resin A) and 0.6% wt (resin B). It was found that the addition of Gr-NAN had no effect on the curing enthalpy and T_g of the binfunctional epoxy A, while it increased both parameters in the case of the multifunctional epoxy B indicating higher degree of curing and crosslinking density. The graphene/epoxy resin mixtures were used to impregnate unidirectional CF tapes. These prepregs were stacked (seven plies) and cured to produce laminates. Interlaminar fracture toughness tests on laminates demonstrated an increase in the initial G_{IC} by 56.3% in epoxy B due to the addition of Gr-NAN. The increase in G_{IC} was only 8.3% in epoxy A contained Gr-NAN while a decrease of 11.1% in epoxy A contained Gr-AVA. Shear lap-joint specimens were prepared using Gr-NAN/CF/epoxy laminates as adherents and two different polyurethane adhesives. A significant improvement in the lap joint shear strength i.e. from 6 MPa to 21MPa was observed owing to the presence of graphene.

ACKNOWLEDGEMENTS

The research leading to these results has received funding from the European Union Seventh Framework Programme under grant agreement No. 604391 and Horizon 2020 Programme under grant agreement No. 696656 Graphene Flagship

REFERENCES

[1] A. Hallal, A. Elmarakbi, A. Shaito, H. El-Hage, Overview of Composite Materials and Their Automotive Applications, in: Adv. Compos. Mater. Automot. Appl. Struct. Integr. Crashworthiness, 2013: pp. 3–28. doi:10.1002/9781118535288.ch1.

[2] A.I. Taub, A.A. Luo, Advanced lightweight materials and manufacturing processes for automotive applications, MRS Bull. 40 (2015) 1045–1053. doi:10.1557/mrs.2015.268.

[3] R. Huang, M. Riddle, D. Graziano, J. Warren, S. Das, S. Nimbalkar, J. Cresko, E. Masanet, Energy and emissions saving potential of additive manufacturing: the case of lightweight aircraft components, J. Clean. Prod. 135 (2016) 1559–1570. doi:10.1016/j.jclepro.2015.04.109.

[4] P.D. Mangalgiri, Composite materials for aerospace applications, Bull. Mater. Sci. 22 (1999) 657–664. doi:10.1007/BF02749982.

[5] A.P. Mouritz, E. Gellert, P. Burchill, K. Challis, Review of advanced composite structures for naval ships and submarines, Compos. Struct. 53 (2001) 21–24. doi:10.1016/S0263-8223(00)00175-6.

[6] C. Smith, Design of Marine Structures in Composite Materials, Elsevier Appl. Sci. Oxford. (1990).

[7] L. Van Den Einde, L. Zhao, F. Seible, Use of FRP composites in civil structural applications, in: Constr. Build. Mater., 2003: pp. 389–403. doi:10.1016/S0950-0618(03)00040-0.

[8] M.S. Scholz, J.P. Blanchfield, L.D. Bloom, B.H. Coburn, M. Elkington, J.D. Fuller, M.E. Gilbert, S.A. Muflahi, M.F. Pernice, S.I. Rae, J.A. Trevarthen, S.C. White, P.M. Weaver, I.P. Bond, The use of composite materials in modern orthopaedic medicine and prosthetic devices: A review, Compos. Sci. Technol. 71 (2011) 1791–1803. doi:10.1016/j.compscitech.2011.08.017.

[9] P.K. Mallick, Thermoset–matrix composites for lightweight automotive structures, in: Mater. Des. Manuf. Light. Veh., Elsevier, 2010: pp. 208–231. doi:10.1533/9781845697822.1.208.

[10] W. Callister Jr., D. Rethwisch, Fundamentals of Materials Science and Engineering: An Integrated Approach, 2013. www.wiley.com/college/callister.

[11] D.L. Hunston, R.J. Moulton, N.J. Johnston, W.D. Bascom, matrix Resin Effects in Composite Delamination: Mode I Fracture Aspects, Toughened Compos. (1987) 74–94.

[12] J.P. Davim, P. Reis, Study of delamination in drilling carbon fiber reinforced plastics

(CFRP) using design experiments, Compos. Struct. 59 (2003) 481–487. doi:10.1016/S0263-8223(02)00257-X.

[13] J. Degrieck, W. Van Paepegem, Fatigue Damage Modelling of Fibre-reinforced Composite Materials: Review, Appl. Mech. Rev. 54 (2001) 279–300. doi:10.1115/1.1381395.

[14] Y. Li, H. Zhang, Z. Huang, E. Bilotti, T. Peijs, Graphite Nanoplatelet Modified Epoxy Resin for Carbon Fibre Reinforced Plastics with Enhanced Properties, J. Nanomater. 2017 (2017). doi:10.1155/2017/5194872.

[15] L. Boogh, B. Pettersson, J.A.E. Månson, Dendritic hyperbranched polymers as toughenersfor epoxy resins, Polymer (Guildf). 40 (1999) 2249–2261. doi:10.1016/S0032-3861(98)00464-9.

[16] F.H. Gojny, M.H.G. Wichmann, U. Köpke, B. Fiedler, K. Schulte, Carbon nanotube-reinforced epoxy-composites: Enhanced stiffness and fracture toughness at low nanotube content, Compos. Sci. Technol. 64 (2004) 2363–2371. doi:10.1016/j.compscitech.2004.04.002.

[17] J.N. Coleman, U. Khan, W.J. Blau, Y.K. Gun'ko, Small but strong: A review of the mechanical properties of carbon nanotube-polymer composites, Carbon N. Y. 44 (2006) 1624–1652. doi:10.1016/j.carbon.2006.02.038.

[18] J. Lee, A.F. Yee, Inorganic particle toughening I: Micro-mechanical deformations in the fracture of glass bead filled epoxies, Polymer (Guildf). 42 (2001) 577–588. doi:10.1016/S0032-3861(00)00397-9.

[19] Y. Tang, L. Ye, Z. Zhang, K. Friedrich, Interlaminar fracture toughness and CAI strength of fibre-reinforced composites with nanoparticles - A review, Compos. Sci. Technol. 86 (2013) 26–37. doi:10.1016/j.compscitech.2013.06.021.

[20] S. Sprenger, M.H. Kothmann, V. Altstaedt, Carbon fiber-reinforced composites using an epoxy resin matrix modified with reactive liquid rubber and silica nanoparticles, Compos. Sci. Technol. 105 (2014) 86–95. doi:10.1016/j.compscitech.2014.10.003.

[21] A.C. Ferrari, F. Bonaccorso, V. Fal'ko, K.S. Novoselov, S. Roche, P. Bøggild, S. Borini, F.H.L. Koppens, V. Palermo, N. Pugno, J.A. Garrido, R. Sordan, A. Bianco, L. Ballerini, M. Prato, E. Lidorikis, J. Kivioja, C. Marinelli, T. Ryhänen, A. Morpurgo, J.N. Coleman, V. Nicolosi, L. Colombo, A. Fert, M. Garcia-Hernandez, A. Bachtold, G.F. Schneider, F. Guinea, C. Dekker, M. Barbone, Z. Sun, C. Galiotis, A.N. Grigorenko, G. Konstantatos, A. Kis, M. Katsnelson, L. Vandersypen, A. Loiseau, V. Morandi, D. Neumaier, E. Treossi, V. Pellegrini, M. Polini, A. Tredicucci, G.M.

Williams, B. Hee Hong, J.-H. Ahn, J. Min Kim, H. Zirath, B.J. van Wees, H. van der Zant, L. Occhipinti, A. Di Matteo, I.A. Kinloch, T. Seyller, E. Quesnel, X. Feng, K. Teo, N. Rupesinghe, P. Hakonen, S.R.T. Neil, Q. Tannock, T. Löfwander, J. Kinaret, Science and technology roadmap for graphene, related two-dimensional crystals, and hybrid systems, Nanoscale. 7 (2015) 4598–4810. doi:10.1039/C4NR01600A.

[22] P.G. Karagiannidis, S.A. Hodge, L. Lombardi, F. Tomarchio, N. Decorde, S. Milana, I. Goykhman, Y. Su, S.V. Mesite, D.N. Johnstone, R.K. Leary, P.A. Midgley, N.M. Pugno, F. Torrisi, A.C. Ferrari, Microfluidization of Graphite and Formulation of Graphene-Based Conductive Inks, ACS Nano. 11 (2017). doi:10.1021/acsnano.6b07735.

[23] K.R. Paton, E. Varrla, C. Backes, R.J. Smith, U. Khan, A. O'Neill, C. Boland, M. Lotya, O.M. Istrate, P. King, T. Higgins, S. Barwich, P. May, P. Puczkarski, I. Ahmed, M. Moebius, H. Pettersson, E. Long, J. Coelho, S.E. O'Brien, E.K. McGuire, B.M. Sanchez, G.S. Duesberg, N. McEvoy, T.J. Pennycook, C. Downing, A. Crossley, V. Nicolosi, J.N. Coleman, Scalable production of large quantities of defect-free few-layer graphene by shear exfoliation in liquids, Nat. Mater. 13 (2014) 624–630. doi:10.1038/nmat3944.

[24] J. Wang, K.K. Manga, Q. Bao, K.P. Loh, High-yield synthesis of few-layer graphene flakes through electrochemical expansion of graphite in propylene carbonate electrolyte, J. Am. Chem. Soc. 133 (2011) 8888–8891. doi:10.1021/ja203725d.

[25] X. Wang, J. Jin, M. Song, An investigation of the mechanism of graphene toughening epoxy, Carbon N. Y. (2013). doi:10.1016/j.carbon.2013.08.032.

[26] D.R. Bortz, E.G. Heras, I. Martin-Gullon, Impressive fatigue life and fracture toughness improvements in graphene oxide/epoxy composites, Macromolecules. (2012). doi:10.1021/ma201563k.

[27] Y. Zhang, Y. Wang, J. Yu, L. Chen, J. Zhu, Z. Hu, Tuning the interface of graphene platelets/epoxy composites by the covalent grafting of polybenzimidazole, Polym. (United Kingdom). 55 (2014) 4990–5000. doi:10.1016/j.polymer.2014.07.045.

[28] J. Kim, J. Kim, S. Song, S. Zhang, J. Cha, K. Kim, H. Yoon, Y. Jung, K.W. Paik, S. Jeon, Strength dependence of epoxy composites on the average filler size of non-oxidized graphene flake, Carbon N. Y. (2017). doi:10.1016/j.carbon.2016.11.023.

[29] C. Kostagiannakopoulou, T.H. Loutas, G. Sotiriadis, A. Markou, V. Kostopoulos, On the interlaminar fracture toughness of carbon fiber composites enhanced with graphene nano-species, Compos. Sci. Technol. 118 (2015) 217–225.

doi:10.1016/j.compscitech.2015.08.017.

[30] H. Ning, J. Li, N. Hu, C. Yan, Y. Liu, L. Wu, F. Liu, J. Zhang, Interlaminar mechanical properties of carbon fiber reinforced plastic laminates modified with graphene oxide interleaf, Carbon N. Y. (2015). doi:10.1016/j.carbon.2015.04.054.

[31] A. Kumar, S. Roy, Characterization of mixed mode fracture properties of nanographene reinforced epoxy and Mode I delamination of its carbon fiber composite, Compos. Part B Eng. (2018). doi:10.1016/j.compositesb.2017.09.052.

[32] R.D. Adams, Adhesive bonding: Science, technology and applications, 2005. doi:10.1533/9781845690755.

[33] E.M. Petrie, Handbook of Adhesives and Sealants, McGraw-Hill, 2000.

[34] D. De Cicco, Z. Asaee, F. Taheri, Use of Nanoparticles for Enhancing the Interlaminar Properties of Fiber-Reinforced Composites and Adhesively Bonded Joints—A Review, Nanomaterials. 7 (2017) 360. doi:10.3390/nano7110360.

[35] M.A. Raza, A.V.K. Westwood, A.P. Brown, C. Stirling, Texture, transport and mechanical properties of graphite nanoplatelet/silicone composites produced by three roll mill, Compos. Sci. Technol. 72 (2012) 467–475. doi:10.1016/j.compscitech.2011.12.010.

[36] Y. Li, H. Zhang, H. Porwal, Z. Huang, E. Bilotti, T. Peijs, Mechanical, electrical and thermal properties of in-situ exfoliated graphene/epoxy nanocomposites, Compos. Part A Appl. Sci. Manuf. (2017). doi:10.1016/j.compositesa.2017.01.007.

[37] D. Yang, A. Velamakanni, G. Bozoklu, S. Park, M. Stoller, R.D. Piner, S. Stankovich, I. Jung, D.A. Field, C.A. Ventrice, R.S. Ruoff, Chemical analysis of graphene oxide films after heat and chemical treatments by X-ray photoelectron and Micro-Raman spectroscopy, Carbon N. Y. 47 (2009) 145–152. doi:10.1016/j.carbon.2008.09.045.

[38] S. Drewniak, R. Muzyka, A. Stolarczyk, T. Pustelny, M. Kotyczka-Morańska, M. Setkiewicz, Studies of Reduced Graphene Oxide and Graphite Oxide in the Aspect of Their Possible Application in Gas Sensors, Sensors. 16 (2016) 103. doi:10.3390/s16010103.

[39] K. Haubner, J. Murawski, P. Olk, L.M. Eng, C. Ziegler, B. Adolphi, E. Jaehne, The route to functional graphene oxide, ChemPhysChem. 11 (2010) 2131–2139. doi:10.1002/cphc.201000132.

[40] F.L. Jin, X. Li, S.J. Park, Synthesis and application of epoxy resins: A review, J. Ind. Eng. Chem. 29 (2015) 1–11. doi:10.1016/j.jiec.2015.03.026.

[41] C. Aouf, H. Nouailhas, M. Fache, S. Caillol, B. Boutevin, H. Fulcrand, Multi-

functionalization of gallic acid. Synthesis of a novel bio-based epoxy resin, in: Eur. Polym. J., 2013: pp. 1185–1195. doi:10.1016/j.eurpolymj.2012.11.025.

[42] S. Chandrasekaran, N. Sato, F. Tölle, R. Mülhaupt, B. Fiedler, K. Schulte, Fracture toughness and failure mechanism of graphene based epoxy composites, Compos. Sci. Technol. 97 (2014) 90–99. doi:10.1016/j.compscitech.2014.03.014.

[43] E.A. Turi, Thermal characterization of polymeric materials, Acad. Press. Brooklyn, New York. (1977) 1977.

[44] E.C. Vouvoudi, I.D. Sideridou, Dynamic mechanical properties of dental nanofilled light-cured resin composites: Effect of food-simulating liquids, J. Mech. Behav. Biomed. Mater. 10 (2012) 87–96. doi:10.1016/j.jmbbm.2012.02.007.

[45] A.R. Kannurpatti, J.W. Anseth, C.N. Bowman, A study of the evolution of mechanical properties and structural heterogeneity of polymer networks formed by photopolymerizations of multifunctional (meth)acrylates, Polymer (Guildf). 39 (1998) 2507–2513. doi:10.1016/S0032-3861(97)00585-5.

[46] H. Lu, L.G. Lovell, C.N. Bowman, Exploiting the heterogeneity of cross-linked photopolymers to create high-Tg polymers from polymerizations performed at ambient conditions, Macromolecules. 34 (2001) 8021–8025. doi:10.1021/ma010542g.

[47] J.F. Dai, G.J. Wang, L. Ma, C.K. Wu, Surface properties of graphene: Relationship to graphene-polymer composites, Rev. Adv. Mater. Sci. 40 (2015) 60–71.

[48] T.D. Chang, J.O. Brittain, Studies of epoxy resin systems: Part D: Fracture toughness of an epoxy resin: A study of the effect of crosslinking and sub -Tg aging, Polym. Eng. Sci. 22 (1982) 1228–1236. doi:10.1002/pen.760221809.

[49] R.A. Pearson, A.F. Yee, Toughening mechanisms in elastomer-modified epoxies - Part 3 The effect of cross-link density, J. Mater. Sci. 24 (1989) 2571–2580. doi:10.1007/BF01174528.

[50] A.C. Garg, Y.W. Mai, Failure mechanisms in toughened epoxy resins-A review, Compos. Sci. Technol. 31 (1988) 179–223. doi:10.1016/0266-3538(88)90009-7.

[51] L.C. Tang, Y.J. Wan, D. Yan, Y.B. Pei, L. Zhao, Y.B. Li, L. Bin Wu, J.X. Jiang, G.Q. Lai, The effect of graphene dispersion on the mechanical properties of graphene/epoxy composites, Carbon N. Y. 60 (2013) 16–27. doi:10.1016/j.carbon.2013.03.050.

[52] N.T. Kamar, M.M. Hossain, A. Khomenko, M. Haq, L.T. Drzal, A. Loos, Interlaminar reinforcement of glass fiber/epoxy composites with graphene nanoplatelets, Compos. Part A Appl. Sci. Manuf. 70 (2015) 82–92. doi:10.1016/j.compositesa.2014.12.010.

[53] X. Chang, M.F. Ren, T. Li, X. Guo, Evaluation of mechanical behaviour of

unidirectional fibre-reinforced composites considering the void morphology, J. Reinf. Plast. Compos. 36 (2017) 1817–1828. doi:10.1177/0731684417727358.

[54] K. Yu, M. Wang, J. Wu, K. Qian, J. Sun, X. Lu, Modification of the Interfacial Interaction between Carbon Fiber and Epoxy with Carbon Hybrid Materials, Nanomaterials. (2016). doi:10.3390/nano6050089.